$Ti_3C_2T_x$ on copper and nickel foams with improved electrochemical performance produced via solution processing for supercapacitor

Lin Su[1], Guobing Ying[1,*], Lu Liu[1], Fengchen Ma[1], Kaicheng Zhang[1], Chen Zhang[1], Xiang Wang[2], Cheng Wang[1]

[1]*Department of Materials Science and Engineering, College of Mechanics and Materials, Hohai University, Nanjing 211100, China*

[2]*Key Laboratory of Superlight Materials & Surface Technology (Harbin Engineering University), Ministry of Education, Harbin 150001, China*

Abstract

Herein, we demonstrate the fabrication of $Ti_3C_2T_x$ electrodes using solution processing. Two-dimensional (2D) nanometer $Ti_3C_2T_x$ flakes are site-aggregated on copper and nickel foam papers with a reconstituted three-dimensional (3D) structure consisting of overlapping and open-pore 2D flakes. When $Ti_3C_2T_x$ was used as electrochemical capacitor electrodes in 1 M Na_2SO_4 solution, the capacitances were comparable to literature values. There is a quantitative linear relationship between the capacitance and foam thicknesses. Given the process scalability and the morphological control that is possible, these results provide a promising road map for convenient and economical supercapacitors.

Keywords: $Ti_3C_2T_x$, MXene, nickel and copper foam, solution processing, supercapacitor

I. Introduction

Since the discovery of single-layer graphene, which has excellent properties, there has been a groundswell of interest in two-dimensional (2D) materials. To date, the classes of 2D materials that are known include graphene, transition metal dichalcogenides, metal oxides, double-metal hydroxides, and MXenes [1]. In 2011, Naguib *et al.* [2] discovered a new 2D material - 2D graphene-like transition metal carbides or carbonitrides, which are derived by selectively etching the A-element in $M_{n+1}AX_n$ (MAX) phases. The selective etching effect of the HF etching agent on element A in MAX phases yields new materials that have a two-dimensional structure that is similar to the structure of graphene [3,4]. These new materials are called MXenes phase materials and the name corresponds to their respective MAX phase precursors, where M is a transition group metal element, A is a group III or IV element [5,6] and X is C or N [3,7]. The general chemical formula of MXene is $M_{n+1}X_nT_x$, where T represents the active functional groups such as hydroxyl groups, oxygen ions, or fluorine ions linked to the surface of layered $M_{n+1}X_nT_x$ [8,9]. Like selective etching of A from MAX phases, MXenes (e.g., $Zr_3C_2T_x$ and $Hf_3C_2T_x$) can also be fabricated by ternary layered structure $Zr_3Al_3C_5$ and $Hf_3[Al(Si)]_4C_6$. With the development of MXenes, there are potentially many more layered metal carbides and carbonitrides that can be transformed into MXenes [10–13]. MXenes have surface hydrophilicity, metal conductivity, and excellent electrochemical properties, and they are expected to be used for energy storage, catalysis, and adsorption, hydrogen storage, sensors, new polymer-reinforced matrix composites, and many other fields [14–22]. For example, the volume capacitance of 2D $Mo_{1.33}C$ MXene is as high as $1100\,F/cm^3$, which is one of the largest reported capacitance values [23].

At present, the number of different MXene chemicals is about 20. However, the most studied MXene is by far still the first MXene that was found: $Ti_3C_2T_x$. As an electrode material in supercapacitors and lithium battery electrodes, this material has excellent performance. $Ti_3C_2T_x$ has already been proved to be a promising candidate for electrodes in supercapacitors and Li-batteries

*Corresponding authors: tel: +86 25 83787027,
e-mail: yinggb2010@126.com, yinggb001@hhu.edu.cn

because it exhibits capacitances that exceed most previously reported materials [9,24]. In KOH solution, ultrasonic treated $Ti_3C_2T_x$ film has a capacity of 100 F/g [15]. The properties of MXene can also be improved by modifying it. For example, it has been reported that an MXene hydrogel can achieve a volume capacitance of 1500 F/cm^3 [25].

To date, MXene film-like electrodes for supercapacitors and battery applications are mostly prepared either via rolling or filtration [26,27]. To improve electrochemical performance, people are committed to reducing the restacking of 2D nanomaterials. Xia *et al.* [28] produced vertically aligned liquid-crystalline $Ti_3C_2T_x$ and obtained an excellent specific capacitance up to 200 F/g (at 2000 mV/s). Recently, $Ti_3C_2T_x$ films have been made using a simple dropping-mild baking approach with a $Ti_3C_2T_x$ flake suspension to make MXene electrodes with high gravimetric capacitances; the electrode was prepared using solution processing [29]. However, simple dropping may not be a rigorous control for the electrode and further research was needed. Very recently, $Ti_3C_2T_x$ [30], Ti_2CT_x [22], and V_2CT_x [31] films were fabricated into transparent and conductive films via solution processing. Nanometer flakes, which were dispersed as colloidal solutions with the Tyndall phenomenon, were also flexible and collapsible. These provided convenient and economical MXene electrodes produced via a large solution process for energy storing applications.

Herein, we investigate the electrochemistry performance of $Ti_3C_2T_x$ electrodes in which $Ti_3C_2T_x$ nanometer flakes site-aggregated on copper and nickel foam papers using a solution process. The effects of the $Ti_3C_2T_x$ electrode substrates (i.e., copper and nickel foam papers) on the performance are also discussed. It is demonstrated that $Ti_3C_2T_x$ electrodes achieve a high capacitance performance and that the substrates play a significant role in the performance.

II. Experimental details

To produce $Ti_3C_2T_x$ colloidal solutions, we first fabricated precursor Ti_3AlC_2 powders. Ti_2AlC powders (−325 mesh, 98 wt.% pure [32]) were mixed with TiC (2–4 μm, 99 wt.% pure, Aladdin Industrial Co., China) in a 1 : 1 ratio for 24 h. The mixed powders were precompacted under a pressure of 30 MPa and then heated to 1350 °C at a heating rate of 10 °C/min followed by a 2 h soak to yield phase-pure Ti_3AlC_2. The resulting sintered Ti_3AlC_2 brick was ground into powder with a drilling bit and passed through a −325 mesh sieve. Ti_3AlC_2 powder (1 g) was then slowly added into a premixed solution containing 1 g of lithium fluoride (LiF, 99 wt.% pure, Shanghai Macklin Biochemical Co., Ltd., China) and 10 ml of 12 M hydrochloric acid (HCl, AR, Shanghai Lingfeng Chemical Reagent Co., China). It was corroded for 24 h at 35 °C. The multilayer $Ti_3C_2T_x$ was washed with deionized water and centrifuged to

separate the reaction product from the supernatant until the supernatant reached a pH value of approximately 6.

Copper foam paper (thickness of 1.6 mm; density of ~0.4 g/cm^3; Shenzhen Tianchenghe Science and Technology Co., Ltd., China) and nickel foam paper (thicknesses of 0.5 mm, 1 mm, 1.6 mm, and 2 mm; density of 0.3–0.5 g/cm^3; Shenzhen Tianchenghe Science and Technology Co., Ltd., China) were used as working electrode matrices; they were cut into square pieces with dimensions of 4 × 4 mm. The sheets were washed with deionized water three times for 15 min each time, and then the sheets were dried and weighed. Each piece of foam sheet was soaked in 12.5 mg/ml $Ti_3C_2T_x$ colloidal solution for site aggregation for 20 s. $Ti_3C_2T_x$ nanometer flakes were dispersed into foam pores via solution processing, and then they were forced coated on the foam via vacuum pressure difference in a vacuum chamber for 4 h. Before solution processing, the solid content of the $Ti_3C_2T_x$ colloidal solution was determined by vacuum filtering a given colloidal solution volume. Finally, after complete vacuum drying, it was weighed.

The samples were characterized by using X-ray diffraction (Rigaku Smartlab) with Cu Kα radiation with a step size of 0.02°° and a speed 3°/min. Microstructures of the samples were observed using a scanning electron microscope (SEM, S-3400N, HITACHI). All electrochemical performances were assessed using a CHI-660 electrochemical workstation (Chenhua Instruments Co., Shanghai, China). Cyclic voltammetry was conducted in three-electrode plastic Swagelok cells. Nickel or copper foam papers coated with $Ti_3C_2T_x$ nanometer flakes were used as working electrodes, and activated carbon was used as a counter electrode. A platinum plate and gold plate with a surface area of about 0.785 cm^2 were used as counter electrodes, and saturated sodium sulphate solution was used as a reference electrode. Pre-cycling of 20 mV/s was performed before the cells were tested at scan rates from 2 mV/s to 100 mV/s in 1 mol/l Na_2SO_4 solution at room temperature. Over the range of 10 mHz to 100 kHz, the same 3-electrode cell configuration described above was used for electrochemical impedance spectroscopy (EIS) at a potential amplitude of 5 mV. Galvanostatic cycling was carried out at a current density of 10 A/g. Gravimetric capacitance (C_m) values can be calculated from a CV curve using the following equation:

$$C_m = \int \frac{I}{2m \cdot s \cdot \Delta V} \, dV \qquad (1)$$

where C_m is the specific capacitance of the working electrode, I is the response current of the CV curves, m is the mass of active materials loaded in the working electrode, s is the scan rate, and ΔV is the potential window. Gravimetric capacitance values can also be determined from the discharge curves according to the following equation:

$$C_m = \frac{I \cdot \Delta t}{m \cdot \Delta V} \qquad (2)$$

where I, Δt, ΔV, and m are respectively the discharge current, discharge time, potential window, and mass of active materials loaded in the working electrode.

III. Results and discussion

A typical XRD pattern (Fig. 1) of Ti_3AlC_2 indicates that the precursor of $Ti_3C_2T_x$ is a phase pure. After etching with LiF+HCl solution, the diffractogram of MXene $Ti_3C_2T_x$ is typical in that the (000l) peaks are down-shifted in 2θ, where the c-lattice parameter (c-LP) of these $Ti_3C_2T_x$ is 27.76 Å, which is considerably larger than the values obtained when $Ti_3C_2T_x$ was etched in
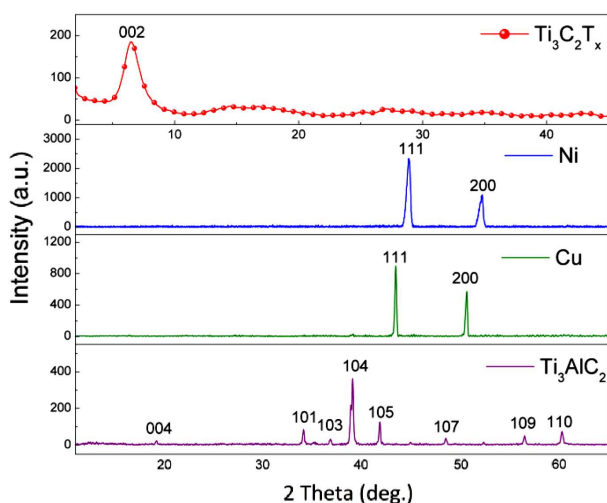
Figure 1. XRD patterns of Ti_3AlC_2, copper foam, nickel foam, and $Ti_3C_2T_x$ (produced by etching Ti_3AlC_2 with LiF + HCl solution)

10% HF. When $Ti_3C_2T_x$ was etched in 10% HF, the c-lattice parameters are closer to ~20 Å [27]. As seen in Fig. 1, typical peaks of pure Ni and Cu with 111 and 200 diffractions are also found for both the nickel and copper foams.

SEM micrographs of nickel and copper foam electrodes or/and those with site-aggregated $Ti_3C_2T_x$ are shown in Fig. 2. In Figs. 2a and 2d, the nickel and copper foams appear to be quite three-dimensional (3D) and net-like porous with pore size of ~200 μm. At low magnification, (Figs. 2b and 2e), the 2D $Ti_3C_2T_x$ flakes have been site-aggregated with lateral pores, and foam substrates presented to be films Figures 2c and 2f show the higher magnification micrographs and confirming nanoflake nature of the collected 2D $Ti_3C_2T_x$ flakes. These observations indicate that the $Ti_3C_2T_x$ nanometer flakes were site-aggregated on the copper and nickel foam papers in the solution processing. The surface energy of the $Ti_3C_2T_x$ nanometer flakes supports the overlapping, which is consistent with transparent and conductive films, or filtration electrodes. With etching of LiF + HCl solution, the mesh held by the surface tension of $Ti_3C_2T_x$ nanometer flakes in aqueous solution results in large flakes.

Electrode mass-normalized cyclic voltammograms of the electrodes produced by site-aggregated $Ti_3C_2T_x$ flakes on 0.5, 1.0, 1.6, and 2.0 mm-thick nickel foam, and 2.0 mm-thick copper foam are shown in Fig. 3. The electrochemical performances of the as-fabricated electrodes were evaluated using cyclic voltammetry (CV) with a three-electrode plastic Swagelok cell in 1 mol/l Na_2SO_4 solution at room temperature. A notable feature in all of the CV curves is the strong dependence of the anodic peak potentials on the scan rates. At scan rates in the range of 2–100 mV/s, the rectangular and symmet-
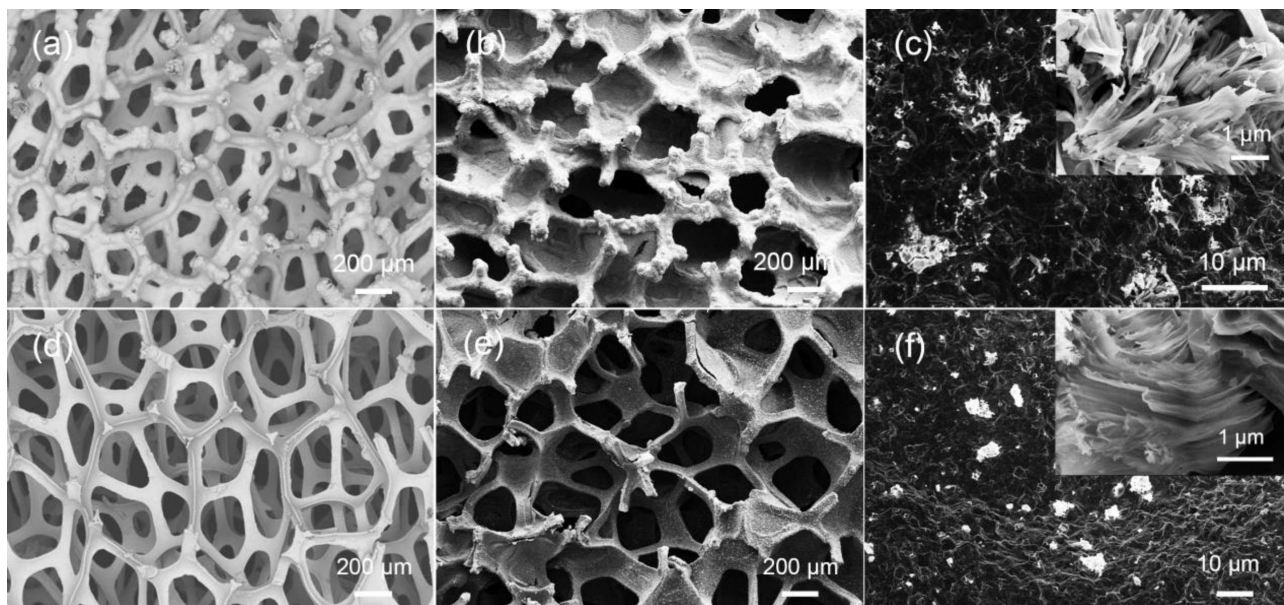
Figure 2. SEM images of: a) nickel foam, b) nickel foam that is site-aggregated with $Ti_3C_2T_x$ flakes, c) $Ti_3C_2T_x$ coating with the inset of nanoflakes, d) copper foam, e) copper foam that is site-aggregated with $Ti_3C_2T_x$ flakes, and f) $Ti_3C_2T_x$ coating with the inset shows nanoflake $Ti_3C_2T_x$ on copper foam
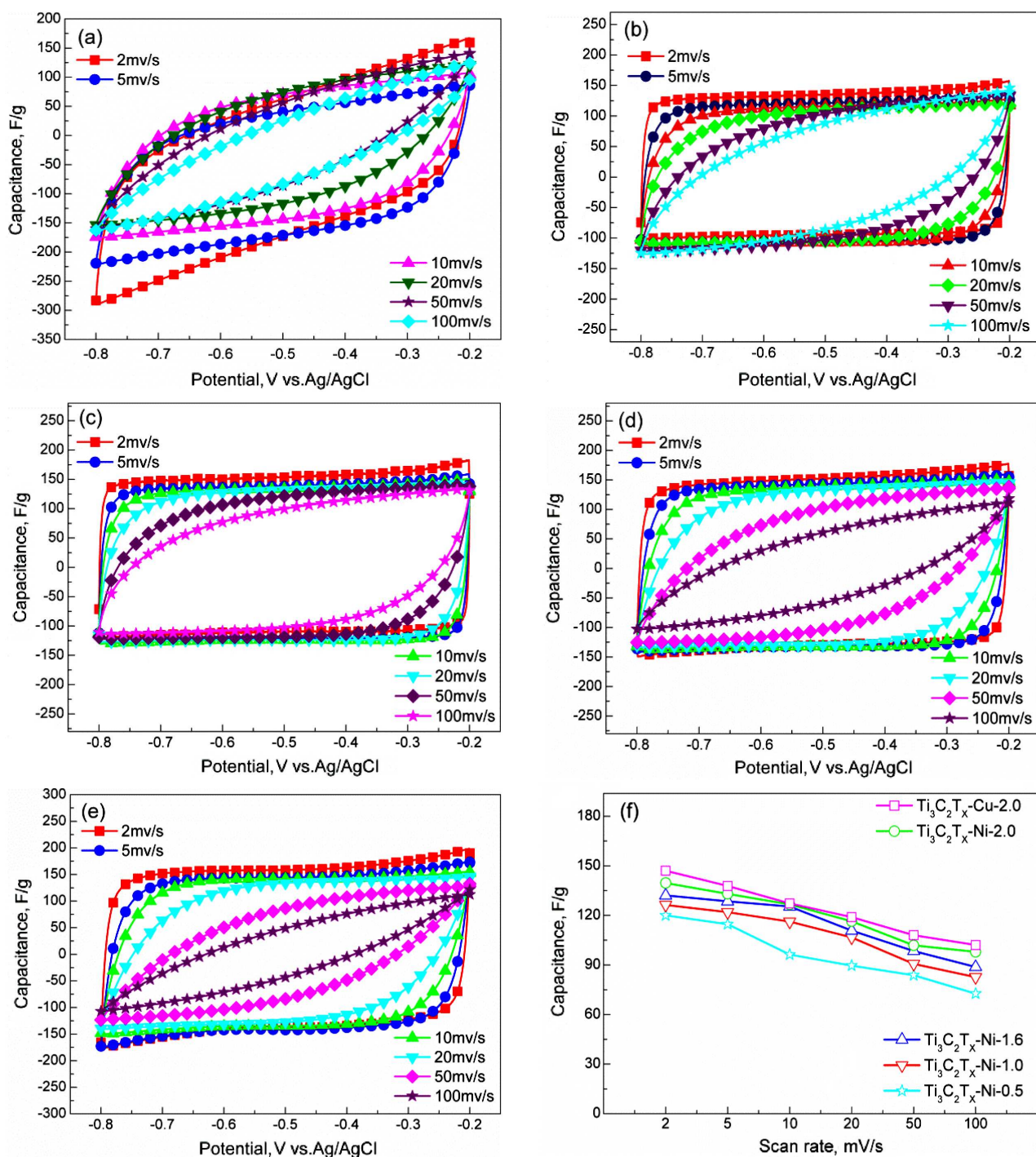
Figure 3. Electrochemical performance of Ti$_3$C$_2$T$_x$ electrodes, i.e. cyclic voltammetry data collected at scan rates from 2 to 100 mV/s for: a) 0.5 mm-thick nickel foam with Ti$_3$C$_2$T$_x$, b) 1.0 mm-thick nickel foam with Ti$_3$C$_2$T$_x$, c) 1.6 mm-thick nickel foam with Ti$_3$C$_2$T$_x$, d) 2.0 mm-thick nickel foam with Ti$_3$C$_2$T$_x$, and e) 2.0 mm-thick copper foam with Ti$_3$C$_2$T$_x$. Scan rate dependence of specific capacitance (f)

ric CV curves of the electrode indicate superior capacitive performance, and the electrode charge storage has strong reversibility. Kinetic analysis of the CV data of the aqueous MXene film was performed to confirm that charge storage is not diffusion-limited as in battery-like electrodes. In contrast, it is most likely pseudocapacitive in nature, as previously reported in the literature regarding Ti$_3$C$_2$T$_x$ and other MXenes [33–35]. However, the curves basically maintain a symmetric rectangular

shape without obvious redox peaks, and this indicates that the pseudocapacitance is not dominant in the electrodes and that their capacities mainly come from the double-layer capacitance between the electrode and the electrolyte interface [36,37]. From a comparison of the areas of each curve, it can be seen that the area of the capacitance curve decreases gradually with an increase in the scan rate, and this is because the ion transmission speed becomes slower with respect to the scan rate. The

ion diffusion not being complete results in a reduced capacitance. When the scan rate reaches 100 mV/s, the curves retain a rectangular shape with a slight distortion. The nickel and copper foams have negligible capacitance because the substrates were covered by $Ti_3C_2T_x$ flakes. In this case, even capacity of bare nickel is negligible compared with that of $Ti_3C_2T_x$ flakes [29]. All of the electrodes, including the foams and MXene films (mass loading of 0.2–0.6 mg), show gravimetric capacitance in the range of 72–146 F/g (Table 1); the specific value depends on the loading of MXene as active material. The gravimetric capacitance values for the films on either nickel and copper foam with the lowest loading was 139 F/g and 146 F/g, respectively.

The dependences of specific capacitances for the site-aggregated $Ti_3C_2T_x$ electrodes on the scan rate (Fig. 3f) show that the gravimetric capacitance values of all of the electrodes are quite similar at all scan rates. Not surprisingly, when the mass loading is lower, the capacitance retention is better. Also, all of the electrodes have comparable decreasing trends with an increase in the scan rate.

Figure 4 shows plots of the 2 mV/s gravimetric capacitance (C_m) as a function of foam thicknesses (h). A least-squares fit of the plot of C_m versus h using our data gives the following formula:
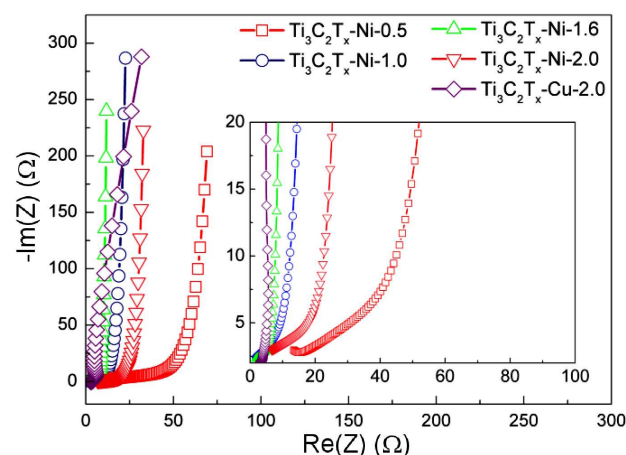
$$C_m = 12.52h + 113.54 \qquad (3)$$
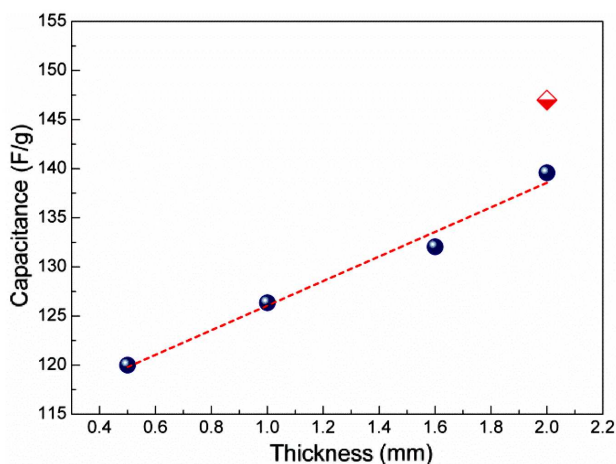
with an R^2 value that is greater than 0.99. Thus, the results show that the gravimetric capacitance increases linearly with an increase in foam thickness. As expected, all of the gravimetric capacitances (Table 1) with scan rates in the range of 2–100 mV/s have the same linear relationship with the foam thickness. Thus, we can conclude that the observed increase is related to the change in specific surface area that results from the change from 2D $Ti_3C_2T_x$ nanoflakes to 3D structures. This can be confirmed from the previous microstructural photographs in which the $Ti_3C_2T_x$ nanoflakes overlap and have open pores. In other words, thick 3D foam structures help to increase the specific surface area of MXene and do not overlap. Note that this is not a circular argument because C_m and h are independent measurements. Moreover, the gravimetric capacitance of the $Ti_3C_2T_x$ electrode that is site-aggregated on the copper foam substrate is higher than that of the electrode on the nickel foam substrate (Fig. 4). This indicates that better conductivity of the electrode promotes the capacitance.

Electrochemical impedance spectroscopy (EIS) was used to understand the ion transport behaviour and the resistance of the electrode; the results are shown in Fig. 5. When the electrode is in contact with the sodium sulphate electrolyte, capacitance-type impedance appears over a wide frequency range, and the fast increase in the imaginary part of the low frequency impedance reflects the capacitance storage mechanism. This is consistent with previous reports on conductive 2D titanium carbide 'clay' electrolyte or vacuum-filtered $Ti_3C_2T_x$ hydrogel film. Although the form of the electrode is different,

Figure 4. Dependencies of C_m for 2 mV/s gravimetric capacitances of $Ti_3C_2T_x$ electrodes on foam thicknesses (h) for nickel (round) and copper (diamond) foam substrates (results of least-squares fit for nickel foam has a slope of 12.52 with $R^2 > 0.99$)

Figure 5. Nyquist plots of $Ti_3C_2T_x$ films that are site-aggregated on nickel and copper foams

Table 1. Effects of foam thicknesses and scan rates on capacitance values

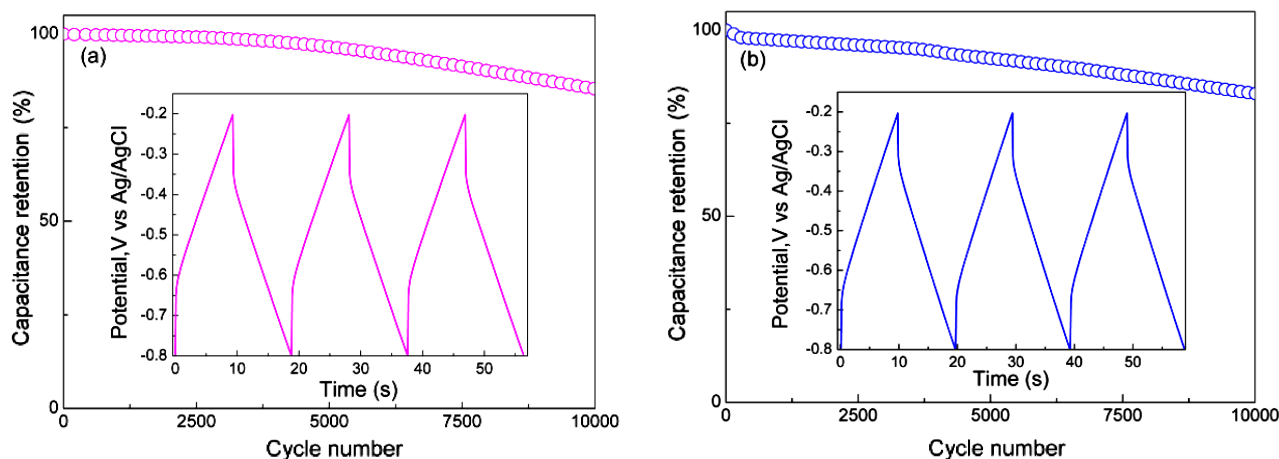| Scan rate [mV/s]	0.5-Ni-$Ti_3C_2T_x$ [F/g]	1-Ni-$Ti_3C_2T_x$ [F/g]	1.6-Ni-$Ti_3C_2T_x$ [F/g]	2-Ni-$Ti_3C_2T_x$ [F/g]	2-Cu-$Ti_3C_2T_x$ [F/g]
2	119	126	132	139	146
5	114	121	128	133	137
10	96	116	125	126	127
20	89	106	110	116	118
50	83	90	98	101	108
100	72	82	88	97	102

Figure 6. Galvanostatic charge-discharge tests conducted at 10 A/g for: a) nickel foam-Ti$_3$C$_2$T$_x$ and b) copper foam-Ti$_3$C$_2$T$_x$

the comparable capacitance impedance over a wide frequency range shows the inherent properties of the same active material in Ti$_3$C$_2$T$_x$.

To explore the cyclability of the prepared electrodes, Ti$_3$C$_2$T$_x$ films that were site-aggregated on both nickel and copper foams were also evaluated, and the results are shown in Figs. 6a and 6b, respectively. Galvanostatic charge-discharge testing at a current density of 10 A/g was also conducted on the site-aggregated Ti$_3$C$_2$T$_x$ electrodes. The voltage *vs.* time profiles have non-triangular shapes (Fig. 6), which are consistent with the pseudocapacitive nature of the charge storage mechanism that is suggested by the corresponding CV curves. The results show that the convenient and economical MXene electrodes formed using this method are promising materials for energy storage applications because these electrodes retained more than 85% of their capacitance after 10 000 cycles. A summary of the specific capacitance and cycling stability obtained for Ti$_3$C$_2$T$_x$ in this work are compared to the values reported in the literature (Table 2). The specific capacitances of the electrodes are

higher than that of many reported Ti$_3$C$_2$T$_x$ electrodes. In some cases, the cycling stabilities are comparable. One of the important factors affecting weight and capacity is the electrolyte. It has been reported that acidic electrolytes are the most beneficial for improving the quality specific capacity of Ti$_3$C$_2$T$_x$ [10,38]. The capacitance of a rolled pure Ti$_3$C$_2$T$_x$ clay electrode can reach up to 900 F/cm^3 in 1 M H$_2$SO$_4$ [27]. The effect of foam thickness on the specific capacitance of the Ti$_3$C$_2$T$_x$ electrode was studied and is discussed in this paper, providing a new idea for the design of supercapacitors. Sodium sulphate, which is a neutral electrolyte, was selected to reduce the effects of electrolyte on the copper and nickel foams. The maximum specific capacity obtained in this paper is 146 F/g, which is about 40% higher than that of other supercapacitors with neutral electrolytes (such as magnesium sulphate [15]). Also important advantages of our electrodes that should not be easily dismissed are the facts that they are nontoxic, low cost and can be produced simply and in large quantities. From this result, it is speculated that the concentration of MXene solu-

Table 2. Effects of foam thicknesses and scan rates on capacitance values

MXene	Specific capacitance [F/g]	Potential window [V]	Capacitance retention [%]	Electrolyte	Ref.
Ti$_3$C$_2$T$_x$-Ni foam	139 (2 mV/s)	[−0.8, −0.2]	85%/10000 cycles	1 M Na$_2$SO$_4$	This work
Ti$_3$C$_2$T$_x$-Cu foam	146 (2 mV/s)	[−0.8, −0.2]	85%/10000 cycles	1 M Na$_2$SO$_4$	This work
Ti$_3$C$_2$T$_x$	120 (2 mV/s)	[−0.4, 0.15]	-	1 M H$_2$SO$_4$	[39]
Ti$_3$C$_2$T$_x$ ionogel film	70 (20 mV/s)	[0, 3]	80%/1000 cycles	[a]EMI-TFSI	[40]
Ti$_3$C$_2$T$_x$ clay	32 (2 mV/s)	[−0.8, 1.0]	-	[b]EMITFSI - AN	[41]
Ti$_3$C$_2$T$_x$/carbon black-PTFE	112 (5 mV/s)	[−0.9, −0.4]	97%/10000 cycles	1 M KOH	[42]
d-Ti$_3$C$_2$T$_x$ paper	122 (5 mV/s)	[−0.6, 0]	-	1 M KOH	[15]
d-Ti$_3$C$_2$T$_x$ film	140 (5 mV/s)	[0, 0.5]	100%/10000 cycles	1 M KOH	[43]
Ti$_3$C$_2$T$_x$ paper	130 (2 mV/s)	[−0.6, 0]	100%/10000	1 M KOH	[15]
Ti$_3$C$_2$T$_x$ paper	120 (2 mV/s)	[−0.6, 0]	-	1 M NaOAc	[15]
Ti$_3$C$_2$T$_x$ paper	100 (2 mV/s)	[−0.6, 0]	-	1 M Na$_2$SO$_4$	[15]
Ti$_3$C$_2$T$_x$ clay	245 (2 mV/s)	[−0.35, 0.2]	100%/10000	1 M H$_2$SO$_4$	[27]
A macroporous Ti$_3$C$_2$T$_x$ film	210 (10 mV/s)	[−1.1, −0.2]	-	3 M H$_2$SO$_4$	[25]

[a]EMI-TFSI: 1-ethyl-3-methylimidazolium bis(trifluoromethylsulfonyl)imide neat ionic liquid.

[b]1 M EMITFSI in AN: 1 M solution of (1-ethyl-3-methylimidazolium bis(trifluoromethylsulfonyl)imide, Solvionic) in acetonitrile (Acros Organics).

tion, diffusion kinetics, and MXene films structures and thicknesses when compared to those of aqueous films introduce changes in the cyclability; thus, future studies are needed to clarify the relative roles.

IV. Conclusions

Herein, 12.5 mg/ml aqueous colloidal solutions of the MXene $Ti_3C_2T_x$ were site-aggregated on both nickel and copper foams via solution processing and used in supercapacitor electrodes. After reconstructing 3D electrodes based on nickel and copper foams, the nanometer flake 2D $Ti_3C_2T_x$ microstructures were studied. Electrochemical performance of the $Ti_3C_2T_x$ electrodes was studied over the scan rate range of 2–100 mV/s using 1 M sodium sulphate as the electrolyte. With a coefficient of 12.52 F/(g mm), the gravimetric capacitance increased linearly with an increase in the foam thickness. Also, better conductivity of the 3D copper substrate resulted in higher capacitance. The gravimetric capacitance values of the 3D $Ti_3C_2T_x$ electrodes and their capacitance retention rates after ten thousand cycles were comparable to many values reported in the literature for the same material.

References

1. K.S. Novoselov, A.K. Geim, S.V. Morozov, D. Jiang, Y. Zhang, S.V. Dubonos, I.V. Grigorieva, A.A. Firsov, "Electric field effect in atomically thin carbon films", *Science*, **306** [5696] (2004) 666–669.
2. M. Naguib, K. Murat, P. Volker, L. Jun, N. Junjie, H. Min, H. Lars, G. Yury, M.W. Barsoum, "Two-dimensional nanocrystals produced by exfoliation of Ti_3AlC_2", *Adv. Mater.*, **23** [37] (2011) 4248–4253.
3. M. Naguib, O. Mashtalir, J. Carle, V. Presser, J. Lu, L. Hultman, Y. Gogotsi, M.W. Barsoum, "Two-dimensional transition metal carbides", *ACS Nano*, **6** [2] (2012) 1322–1331.
4. A.L. Ivanovskii, A.N. Enyashin, "Graphene-like transition-metal nanocarbides and nanonitrides", *Russ. Chem. Rev.*, **82** [8] (2013) 735–746.
5. A. Zhou, L.I. Zhengyang, L.I. Liang, L. Wang, L.I. Shangsheng, "Preparation and microstructure of Ti_3SiC_2 bonded cubic boron nitride superhard composites", *J. Chin. Ceram. Soc.*, **42** [2] (2014) 220–224.
6. M.W. Barsoum, T. El-Raghy, "The MAX phases: Unique new carbide and nitride materials: Ternary ceramics turn out to be surprisingly soft and machinable, yet also heat-tolerant, strong and lightweight", *Am. Scientist*, **89** [4] (2001) 334–343.
7. P. Eklund, M. Beckers, U. Jansson, H. Högberg, L. Hult-

man, "The $M_{n+1}AX_n$ phases: Materials science and thin-film processing", *Thin Solid Films*, **518** [8] (2010) 1851–1878.
8. X. Zhang, M. Xue, X. Yang, Z. Wang, G. Luo, Z. Huang, X. Sui, C. Li, "Preparation and tribological properties of $Ti_3C_2(OH)_2$ nanosheets as additives in base oil", *RSC Adv.*, **5** [4] (2014) 2762–2767.
9. Q. Tang, Z. Zhou, P. Shen, "Are MXenes promising anode materials for Li ion batteries? Computational studies on electronic properties and Li storage capability of Ti_3C_2 and $Ti_3C_2X_2$ (X = F, OH) monolayer", *J. Am. Chem. Soc.*, **134** [40] (2012) 16909–16924.
10. B. Anasori, M.R. Lukatskaya and Y. Gogotsi, "2D metal carbides nitrides (MXenes) for energy storage", *Nature Rev. Mater.*, **2** [2] (2017) 16098.
11. P. Eklund, J. Rosen, P.O.Å. Persson, "Layered ternary $M_{n+1}A_n$ phases and their 2D derivative MXene: An overview from a thin-film perspective", *J. Phys. D Appl. Phys.*, **50** [11] (2017) 113001.
12. J. Zhou, X. Zha, F.Y. Chen, Q. Ye, P. Eklund, S. Du, Q. Huang., "A two-dimensional zirconium carbide by selective etching of Al_3C_3 from nanolaminated $Zr_3Al_3C_5$", *Angew. Chem. Int. Ed.*, **55** [16] (2016) 5008–5013.
13. J. Zhou, X. Zha, X. Zhou, F. Chen, G. Gao, S. Wang, C. Shen, T. Chen, C. Zhi, P. Eklund, "Synthesis and electrochemical properties of two-dimensional hafnium carbide", *ACS Nano*, **11** [4] (2017) 3841–3850.
14. M. Naguib, J. Come, B. Dyatkin, V. Presser, P.L. Taberna, P. Simon, M.W. Barsoum, Y. Gogotsi, "MXene: A promising transition metal carbide anode for lithium-ion batteries", *Electrochem. Commun.*, **16** [1] (2012) 61–64.
15. M.R. Lukatskaya, O. Mashtalir, C.E. Ren, Y. Dall'Agnese, P. Rozier, P.L. Taberna, M. Naguib, P. Simon, M.W. Barsoum, Y. Gogotsi, "Cation intercalation and high volumetric capacitance of two-dimensional titanium carbide", *Science*, **341** [6153] (2013) 1502–1505.
16. Y. Yoon, K. Lee, H. Lee, "Low-dimensional carbon and MXene-based electrochemical capacitor electrodes", *Nanotechnol.*, **27** [17] (2016) 172001.
17. X. Li, G. Fan, C. Zeng, "Synthesis of ruthenium nanoparticles deposited on graphene-like transition metal carbide as an effective catalyst for the hydrolysis of sodium borohydride", *Int. J. Hydrogen Energy*, **39** [27] (2014) 14927–14934.
18. Q. Peng, G. Jianxin, Z. Qingrui, X. Jianyong, L. Baozhong, Z. Aiguo, L. Riping, T. Yongjun, "Unique lead adsorption behavior of activated hydroxyl group in two-dimensional titanium carbide", *J. Am. Chem. Soc.*, **136** [11] (2014) 4113–4116.
19. O. Mashtalir, K.M. Cook, V. Mochalin, M. Crowe, M.W. Barsoum, Y. Gogotsi, "Dye adsorption and decomposition on two-dimensional titanium carbide in aqueous media", *J. Mater. Chem. A*, **2** [35] (2014) 14334–14338.
20. Q. Hu, S. Dandan, W. Qinghua, W. Haiyan, W. Libo, L. Baozhong, Z. Aiguo, H. Julong, "MXene: a new family of promising hydrogen storage medium", *J. Phys. Chem. A*, **117** [51] (2013) 14253–14260.
21. Z. Ling, C.E. Ren, Z. Meng-Qiang, Y. Jian, J.M. Giammarco, Q. Jieshan, M.W. Barsoum, G. Yury, "Flexible and conductive MXene films and nanocomposites with high capacitance", *Proc. National Academy of Science*, **111** [47] (2014) 16676–16681.
22. G. Ying, A.D. Dillon, A.T. Fafarman, M.W. Barsoum, "Transparent, conductive solution processed spincast 2D

Ti_2CT_x (MXene) films", *Mater. Res. Lett.*, **5** [6] (2017) 391–398.

23. Q. Tao, M. Dahlqvist, J. Lu, S. Kota, R. Meshkian, J. Halim, J. Palisaitis, L. Hultman, M.W. Barsoum, P.O.Å. Persson, "Two-dimensional $Mo_{1.33}C$ MXene with divacancy ordering prepared from parent 3D laminate with in-plane chemical ordering", *Nature Commun.*, **8** (2017) 14949–14955.

24. D. Sun, M. Wang, Z. Li, G. Fan, L. Fan, A. Zhou, "Two-dimensional Ti_3C_2 as anode material for Li-ion batteries", *Electrochem. Commun.*, **47** [10] (2014) 80–83.

25. M.R. Lukatskaya, S. Kota, Z. Lin, M.Q. Zhao, N. Shpigel, M.D. Levi, J. Halim, P.L. Taberna, M.W. Barsoum, P. Simon, "Ultra-high-rate pseudocapacitive energy storage in two-dimensional transition metal carbides", *Nature Energy*, **2** [8] (2017) 17105–17116.

26. M.Q. Zhao, C.E. Ren, L. Zheng, M.R. Lukatskaya, Z. Chuanfang, K.L.V. Aken, M.W. Barsoum, G. Yury, "Flexible MXene/carbon nanotube composite paper with high volumetric capacitance", *Adv. Mater.*, **27** [2] (2014) 339–345.

27. M. Ghidiu, M.R. Lukatskaya, M.Q. Zhao, Y. Gogotsi, M.W. Barsoum, "Conductive two-dimensional titanium carbide 'clay' with high volumetric capacitance", *Nature*, **516** [7529] (2014) 78–81.

28. Y. Xia, T.S. Mathis, M.Q. Zhao, B. Anasori, A. Dang, Z. Zhou, H. Cho, Y. Gogotsi, S. Yang, "Thickness-independent capacitance of vertically aligned liquid-crystalline MXenes", *Nature*, **557** (2018) 409–412.

29. M. Hu, L. Zhaojin, Z. Hui, H. Tao, Z. Chao, W. Zhen, W. Xiaohui, "Self-assembled $Ti_3C_2T_x$ MXene film with high gravimetric capacitance", *Chem. Commun.*, **51** [70] (2015) 13531–13533.

30. A.D. Dillon, M.J. Ghidiu, A.L. Krick, J. Griggs, S.J. May, Y. Gogotsi, M.W. Barsoum, A.T. Fafarman, "Highly conductive optical quality solution-processed films of 2D titanium carbide", *Adv. Funct. Mater.*, **26** [23] (2016) 4162–4168.

31. G. Ying, S. Kota, A.D. Dillon, A.T. Fafarman, M.W. Barsoum, "Conductive transparent V_2CT_x (MXene) films", *Flatchem*, **8** (2018) 25–30.

32. G. Ying, B. Tian, X. He, S. Du, P. Wang, C. Wang, Y. Wu, "Influence of heat treatment on the microstructure and properties of Ti_2AlC by SHS/PHIP", *Rare Metal Mater. Eng.*, **44** (2015) 340–344.

33. P. Collini, S. Kota, A.D. Dillon, M.W. Barsoum, A.T. Fafarman, "Electrophoretic deposition of two-dimensional titanium carbide (MXene) thick films", *J. Electrochem. Soc.*, **164** [9] (2017) 573–580.

34. M.R. Lukatskaya, S.M. Bak, X. Yu, X.Q. Yang, M.W. Barsoum, Y. Gogotsi, "Probing the mechanism of high capacitance in 2D titanium carbide using in situ X-ray absorption spectroscopy", *Adv. Energy Mater.*, **5** [15] (2015) 1500589.

35. M. Hu, Z. Li, T. Hu, S. Zhu, C. Zhang, X. Wang, "High-capacitance mechanism for $Ti_3C_2T_x$ MXene by in situ electrochemical Raman spectroscopy investigation", *ACS Nano*, **10** [12] (2016) 11344–11350.

36. C. Costentin, T.R. Porter, J.M. Savéant, "How do pseudo-capacitors store energy? Theoretical analysis and experimental illustration", *ACS Appl. Mater. Interf.*, **9** [10] (2017) 8649–8658.

37. P. Simon, Y. Gogotsi, B. Dunn, "Where do batteries end and supercapacitors begin?", *Science*, **343** [6176] (2014) 1210–1211.

38. V.M.H. Ng, H. Huang, K. Zhou, P.S. Lee, W. Que, Z.J. Xu, L.B. Kong, "Recent progress in layered transition metal carbides and/or nitrides (MXenes) and their composites: synthesis and applications", *J. Mater. Chem. A*, **5** [7] (2017) 3039–3068.

39. O. Mashtalir, M.R. Lukatskaya, A.I. Kolesnikov, E. Raymundo-Piã Ero, M. Naguib, M.W. Barsoum, Y. Gogotsi, "The effect of hydrazine intercalation on the structure and capacitance of 2D titanium carbide (MXene)", *Nanoscale*, **8** [17] (2016) 9128–9133.

40. Z. Lin, D. Barbara, P.L. Taberna, K.L.V. Aken, B. Anasori, Y. Gogotsi, P. Simon, "Capacitance of $Ti_3C_2T_x$ MXene in ionic liquid electrolyte", *J. Power Sources*, **326** (2016) 575–579.

41. Y. Dall Agnese, P. Rozier, P. Taberna, Y. Gogotsi, P. Simon, "Capacitance of two-dimensional titanium carbide (MXene) and MXene/carbon nanotube composites in organic electrolytes", *J. Power Sources*, **306** (2016) 510–515.

42. S.Y. Lin, X. Zhang, "Two-dimensional titanium carbide electrode with large mass loading for supercapacitor", *J. Power Sources*, **294** (2015) 354–359.

43. S. Xu, G. Wei, J. Li, Y. J, N. Klyui, V. Izotov, W. Han, "Binder-free $Ti_3C_2T_x$ MXene electrode film for supercapacitor produced by electrophoretic deposition method", *Chem. Eng. J.*, **317** (2017) 1026–1036.